Chemical Engineering Journal 322 (2017) 73–81

Contents lists available at ScienceDirect

Chemical Engineering Journal

journal homepage: www.elsevier.com/locate/cej

High power supercapacitors based on hierarchically porous sheet-like nanocarbons with ionic liquid electrolytes

Hai Su [a], Haitao Zhang [a,*], Fangyan Liu [a], Fengjun Chun [a], Binbin Zhang [a], Xiang Chu [a], Haichao Huang [a], Weili Deng [a], Bingni Gu [a], Hepeng Zhang [a], Xiaotong Zheng [a], Minhao Zhu [a,b], Weiqing Yang [a,b,*]

[a] Key Laboratory of Advanced Technologies of Materials (Ministry of Education), School of Materials Science and Engineering, Southwest Jiaotong University, Chengdu 610031, PR China
[b] State Key Laboratory of Traction Power, Southwest Jiaotong University, Chengdu 610031, PR China

HIGHLIGHTS

- HPSNCs were obtained by a simply large-scale preparing method.
- Hierarchically porous structure from micro-to-macro-pores are obtained.
- High power density along with high energy density are achieved.
- The HPSNC-based EDLCs show superior cycling stability.

GRAPHICAL ABSTRACT

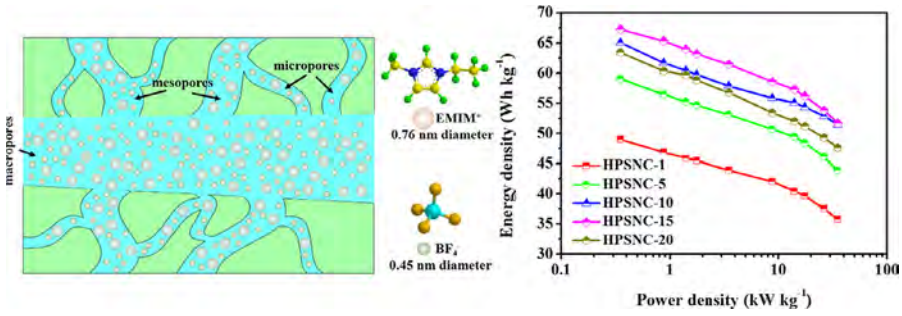

ARTICLE INFO

Article history:
Received 22 December 2016
Received in revised form 31 March 2017
Accepted 1 April 2017
Available online 4 April 2017

Keywords:
Hierarchical structure
Nanocarbons
Graphene
Supercapacitors
Power density
Ionic liquid

ABSTRACT

Supercapacitors with ionic liquid (IL) electrolytes can reach high work voltage and accompanied high energy density, which are the critical parameters for supercapacitors' rapid development. However, supercapacitors with IL electrolytes usually suffer from low power density due to low conductivity, large ionic size and high viscosity of the electrolytes. Herein we reported hierarchically porous sheet-like nanocarbons (HPSNCs) prepared by direct activation of graphene oxide and polytetrafluoroethylene (PTFE) polymer are promising electrode materials for high power supercapacitors with also high energy density. During the activation process, the PTFE particles as a spacer that can effectively hinder the restack of graphene oxide and simultaneously transformed into sheet-like nanocarbons at high temperatures. As a result, the as-prepared samples exhibit highest surface area of ~2000 $m^2 g^{-1}$ and largest pore volume of 1.90 $cm^3 g^{-1}$. Benefit from hierarchically porous structure from micro-to-macro-pores, which largely shorten the diffusion distance of electrolyte ions, the HPSNC electrodes show a high energy density of 51.7 Wh kg^{-1} at a power density of 35 kW kg^{-1} in symmetric supercapacitors with IL electrolyte. In addition, the HPSNC-based supercapacitors also possess an excellent cycling stability with 88% capacitance retention after 5000 cycles. Unambiguously, this work demonstrated the potential of HPSNCs for high power supercapacitors with high energy density and application in integrated energy management electronics.

© 2017 Published by Elsevier B.V.

1. Introduction

Electrochemical double layer capacitors (EDLCs), one kind of supercapacitors, are new energy storage devices that store charge by electrostatic interaction between electrode/electrolyte

* Corresponding authors at: Key Laboratory of Advanced Technologies of Materials (Ministry of Education), School of Materials Science and Engineering, Southwest Jiaotong University, Chengdu 610031, PR China (W. Yang).
E-mail addresses: haitaozhang@swjtu.edu.cn (H. Zhang), wqyang@swjtu.edu.cn (W. Yang).

http://dx.doi.org/10.1016/j.cej.2017.04.012
1385-8947/© 2017 Published by Elsevier B.V.

interfaces. Benefit from unique reversible ion adsorption, they possess high power density (>10 kW kg^{-1}), fast charge/discharge rate (within seconds) and long cycle life (>10^5 cycles). Unfortunately, they usually suffer from relatively low energy density (~6 Wh kg^{-1}), which cannot meet the increasing requirements in portable electronic devices and electric vehicles [1–7]. Therefore, many strategies have been developed to improve its energy density, including (i) enhancing the physicochemical properties like specific surface area (SSA), pore structure, and the electrical conductivity, etc. of a single electrode material [8–11], (ii) structural design and chemical composite of electrode materials with multi-dimensional or micro/nano-structures [12–14], (iii) using the electrolyte with higher work voltage like ionic liquid electrolytes [15–17], and (iv) improving the manufacturing technology of the whole device [18].

Ascribing to much more electrochemical stability of IL electrolytes, the energy density of EDLCs has being considerably improved. For examples, hierarchical porous nitrogen-doped carbon in 1-ethyl-3-methylimidazolium tetrafluoroborate ($EMIMBF_4$) electrolyte possess a high energy density of 59.8 Wh kg^{-1} at a power density of 875 W kg^{-1}, while in 6 M KOH aqueous electrolyte, only exhibits an energy density of 10.3 Wh kg^{-1} at a power density 1.3 kW kg^{-1} [19]. Ma's group demonstrated that the graphene-activated carbon composite had an energy density of 6.1 Wh kg^{-1} in KOH aqueous electrolyte, while in $EMIMBF_4$ electrolyte, the energy density reached up to 52.2 Wh kg^{-1} [20]. Moreover, Tian et al. had reported that a renewable graphene-like nitrogen-doped carbon displayed a maximum energy density of 51 Wh kg^{-1} in the IL mixture of 1-ethyl-3-methylimidazolium bis (trifluoromethylsulfonyl)imide (EMIMTFSI) and $EMIMBF_4$ electrolyte [21]. However, due to their low electrical conductivity, larger ionic size and high viscosity in nature, one typical IL electrolyte $EMIMBF_4$ shows ~1/10 in electrical conductivity comparing to commercial organic electrolyte tetraethylammonium tetrafluoroborate dissolved into acetonitrile solution ($TEABF_4$/AN), the supercapacitors with IL electrolytes usually suffer from low power density, meaning high equivalent series resistance (ESR) and rapid capacitance decline at a high current. Even through incorporating single-walled carbon nanotube with high electrical conductivity into graphene aerogel, the composited carbon aerogel electrodes in $EMIMBF_4$ electrolyte showed a high energy density of 65.6 Wh kg^{-1} along with a low power density of 9.1 kW kg^{-1} [22]. Since the energy density of EDLCs is far from lower than the secondary batteries like Li-ion batteries, the intrinsic advantages of high power and rapid charge-discharge must be maintained.

The power density, to some extent, is limited by the resistance to electronic transmission in porous electrodes and especially by the resistance to ionic current flow in the electrolyte [23]. There will be a confine to the small size of the pores that is related to the accessible pores to the ion from the electrolyte solution. As the average pore size becomes closer to the ion size, the electroadsorption kinetics slows down [24–25]. And the increasing resistance is another factor that is responsible for the commonly observed decline in rate-capability as the total surface area is increased, particularly at large surface area. Hence, it is very important to meet the balance between the pore size and the ion size of the electrolyte that are suitable for EDLCs. Alternatively, developing one kind of electrode material with hierarchical pore structure and high ion-accessible surface area that is helpful to ion transportation is probably to meet the demands of both high energy and high power for EDLCs. The previous works implied that hierarchical porosity design, large pore volume and wide pore size distribution could efficiently improve the ion-accessible surface area and hence leading to high capacitance [8,26–27]. However, these EDLCs in IL electrolytes greatly improve energy density at the sacrifice of high power density. And increasing energy without compromising power is still the topical challenge for supercapacitors [28].

Herein, we present a simply scalable approach to prepare hierarchically porous sheet-like nanocarbons based on direct KOH activation of graphene oxide and PTFE polymer. The obtained hierarchical porous carbon exhibits relatively high SSA (~2000 m^2 g^{-1}), good electric conductivity and excellent electrochemical performance. Moreover, the optimized HPSNCs show abundant of micropores, mesopores and macropores that are beneficial to realize both high energy density and power density. The energy density reaches up to 51.7 Wh kg^{-1} with an extremely high power density of 35 kW kg^{-1} for HPSNC-based symmetric EDLCs with $EMIMBF_4$ electrolyte. In addition, the symmetrical EDLCs also possess long-term cycling stability with 88% retention after 5000 cycles. These observations unambiguously demonstrate the capability of simply large-scale processed HPSNCs as high-performance electrode materials for EDLCs with IL electrolytes, which opens up a new approach for high-performance energy storage.

2. Experimental section

2.1. Materials

Graphite powders (8000 mesh) and 1-ethyl-3-methylimidazolium tetrafluoroborate ($EMIMBF_4$) ionic liquid electrolyte were purchased from Aladdin Industrial Corporation (Shanghai, China). Concentrated sulfuric acid (H_2SO_4), sodium nitrate ($NaNO_3$), potassium permanganate ($KMnO_4$) and hydrogen peroxide (H_2O_2, 30 wt %), hydrochloric acid (HCl) and potassium hydroxide (KOH) were analytical pure grade, which were purchased from Kelong Chemical Reagents Company (Chengdu, China) without further purification. Polytetrafluoroethylene (PTFE, 60 wt% dispersion in water) was purchased from Dakin (Japan). The polypropylene paper separator with a thickness of 20 μm was purchased from NKK Corporation.

2.2. Synthesis of HPSNCs

GO was synthesized by a modified Hummers method [29] and the detailed process is given in Supporting information (SI, Experimental S1). For preparing HPSNCs, in a typical procedure, 50 mg GO was uniformly dispersed into 50 ml deionized water by ultrasonic vibration for 2 h. And then, PTFE emulsion with a mass ratio of 60 wt% was weighed based on the weight ratio of GO to PTFE (from 1:1 to 1:20) and mixed with 20 ml deionized water under magnetic stirred for 5 min. Then, a certain amount of KOH with a weight ratio of 1:6 (KOH to GO and PTFE) was added into the above-obtained solutions and magnetic stirred for 15 min. After GO solution was added, the mixed solution was further agitated for 2 h. Afterwards, the plastic breaker with the solutions was transferred to a water bath kept at 60 °C under continually stirring until obtained solid mixture. After that, the solid mixtures were transferred into the tube furnace (Φ 80 × 1000 mm, BTF-1400C, Anhui BEQ Technology CO., LTD, China) and firstly kept constant at 400 °C for 2 h and followed by reacted at 800 °C for 2 h under Ar atmosphere, and then immerse into enough 2 M HCl aqueous solution for 12 h. Finally, the mixture was washed with deionized water under vacuum filtration and desiccation at 80 °C for 12 h and the obtained samples were denoted as HPSNC-1, HPSNC-5, HPSNC-10, HPSNC-15, and HPSNC-20, respectively.

2.3. Sample characterizations

The morphologies of the as-prepared samples were characterized by a FEI QUANTA FEG 250 scanning electron microscopy

(SEM) and a JEOL JEM-2100F transmission electron microscopy (TEM), respectively. X-ray diffraction (XRD) patterns were obtained on a PANalytical X'Pert Powder diffractometer with Cu Kα radiation between 5 and 80°. Raman spectra measurements were conducted using a RM2000 microscopic confocal Raman spectrometer with a 514 nm laser beam. X-ray photoelectron spectroscopy (XPS) measurements were performed on Thermo Scientific ESCALAB 250Xi. TG and DSC analysis were carried out with NETZSCH STA 449F3. N_2 adsorption/desorption isotherms at −196 °C were carried out with a Micromeritics ASAP 2020 surface area and pore size analyzer, and the specific surface area values and pore size distribution curves were obtained by Brunauer-Emmett-Teller (BET) and density functional theory (DFT) methods, respectively.

2.4. Preparation of EDLC electrodes

In order to prepare the working electrode, 95 wt% of the as-prepared HPSNCs and 5 wt% PTFE binders with a mass ratio of 10 wt% were mixed in isopropyl alcohol. The mixture was placed in an oven at 80 °C to remove excess isopropyl alcohol after blended for 30 min. And then, kneaded thoroughly and rolled down to ~100 μm thick slices. After drying at 120 °C for 24 h, the slices were punched into disk-shaped electrodes with a diameter of 1.2 cm. The loading mass of a single electrode for HPSNC-1, HPSNC-5, HPSNC-10, HPSNC-15 and HPSNC-20 is 3.46 ± 0.04, 2.45 ± 0.05, 2.01 ± 0.08, 1.82 ± 0.03, and 1.55 ± 0.04 mg cm^{-2}, respectively. And the electrode density is 0.30 ± 0.04, 0.21 ± 0.05, 0.17 ± 0.07, 0.17 ± 0.03, 0.15 ± 0.04 g cm^{-3} for HPSNC-1, HPSNC-5, HPSNC-10, HPSNC-15 and HPSNC-20, respectively. Finally, the disk-shaped HPSNC electrodes were pressed onto nickel foam with a thickness of 100 μm.

2.5. Electrochemical measurements

The cyclic voltammetry (CV), galvanostatic charge/discharge (GCD) and electrochemical impedance spectroscopy (EIS) were conducted with a CHI 660E electrochemical workstation (Chenhua, Shanghai, China). The cycling stability was carried out with a LAND cell measurement system. In a three-electrode configuration, 6 M KOH as the aqueous electrolyte, the prepared electrode pressed onto nickel foam current collector (3 cm × 2 cm) as working electrode, a platinum plate (2 cm × 2 cm) as the counter electrode, and a Hg/HgO electrode as the reference electrode. In the two-electrode configuration, 2032 type coin cells were used to assemble symmetric supercapacitors, the electrode pressed onto nickel foam with same diameter, 6 M KOH and $EMIMBF_4$ as the electrolytes, and a polypropylene paper separator was sandwiched between two working electrodes. The parameters like specific capacitance, energy density, and power density are determined in Supporting information (SI, Experimental S2).

3. Results and discussion

The primary advantage of the current process is that it establishes a wide range of micro-to-macroporous sheet-like nanocarbons simply through KOH activation. With the addition of PTFE, the restack of GO after thermal reduction can be alleviated since its function of the spacer. The PTFE polymers fill into the graphene layers and then transformed into stable nanocarbons at high temperatures, which are critical to form hierarchical structure. On the other hand, the reaction of KOH with the carbonized PTFE and GO to form different pore sizes by etching the carbon atoms. The contents of PTFE and KOH show significant effects on the microstructures of the resultants as illustrated by Fig. 1a. Overall, the content of sheet-like nanocarbons increases and the macropores become abundant with increasing the content of PTFE and KOH.

The SEM characterization further verified the effect. It is clear that all the samples possesses highly crumpled morphology and 3D interconnected porous structure formed on the graphene surface, which is attributed to the decomposition of oxygen containing groups and etch of the graphene sheets by KOH (Fig. 1b–f). Interestingly, the amount of KOH and PTFE have influenced on the pore sizes and numbers. In Fig. 1b, the size of pores is very small for HPSNC-1, however, many large pores can be easily observed for HPSNC-5, HPSNC-10, HPSNC-15 (Fig. 1c–e) and the largest pores exist on the HPSNC-20 (Fig. 1f). The evolution of pore structures could on one hand due to the KOH etch reaction on GO, which facilitates the creation of in-plane pores. On the other hand, high content of PTFE in the precursors led to large pores since most PTFE materials were ignited loss at the temperature higher than 550 °C, which was verified by TG-DSC characterization (Fig. S1). Moreover, higher contents of PTFE particles yielded the higher contents of sheet-like nanocarbons that covered on the graphene surface, which can be seen at the whole areas of the samples (SI, Fig. S2a–e). In addition, direct heat-treatment of PTFE without the addition of GO and KOH only yielded particles and layers stacked cluster accompanying with some irregular morphologies (Figs. 1g, S2f and S3). Although hierarchical structures can be prepared by previously reported methods such as templating method or colloidal solution self-assembly, sophisticated designs and processes are usually required for each individual component [30,31]. In contrast, our direct activation method allows the construction of hierarchical porosity using a facile and efficient process.

To further investigate the microstructures of the as-prepared HPSNC samples, the TEM images were collected and presented in Fig. 2. All the samples are consisted with sheet-like morphology, indicating that the sheet-like nanocarbons are successfully prepared through directly activating the mixture of GO and PTFE (Fig. 2a–e). Highly curved and wrinkled graphene sheets and a substantial amount of pores can be observed, which is in accordance with SEM results. As expected, the ratio of sheet-like nanocarbons to curved graphene layers increases with further increasing PTFE. HRTEM also demonstrates that the as-prepared HPSNC-15 sample possesses highly porous structure (Fig. 2f). Since HPSNC samples are produced including KOH activation process, the crystallinity of HPSNC-15 show amorphous structure as indicated by Fig. 2f (HPSNC-1, HPSNC-5, HPSNC-10 and HPSNC-20 are similar, SI, Fig. S4).

Fig. 3a shows the XRD patterns of graphite, GO and the as-prepared HPSNC samples. The diffraction peaks of graphite can be assigned to graphite-2 h (JCPDS 41-1487). Graphite displays a sharp diffraction peak at $2\theta \approx 26.5°$ with an interlayer distance of 0.336 nm according to Bragg equation. After oxidation treatment, a characteristic peak is presented at $2\theta \approx 10.3°$ and the interlayer distance greatly increases to 0.858 nm as the formation of oxygen functional groups between graphite layers [32]. PTFE powders with high crystalline transformed into amorphous nanocarbons after the removal of Fluorine elements by thermal treatment (SI, Fig. S5). Two weak and broad diffraction peaks centered at around 24.6 and 43.0° for all the as-prepared HPSNC samples, which are assigned to the (002) and (100) plane of graphitic layer, respectively [33]. The (002) interlayer spacing of the as-prepared HPSNC samples gradually increases from 0.358 to 0.402 nm with increasing the weight ratio of GO to PTFE (SI, Table S1). These differences demonstrate that PTFE particles locating at the edge and/or center of different graphene layers can alleviate the restack of graphene oxide layers during thermal reduction. Moreover, a larger intensity increases in the low-angle region for HPSNC-15, indicating high porosity [11].

In order to further investigate the structural differences of the as-prepared HPSNC samples with different weight ratios of GO to

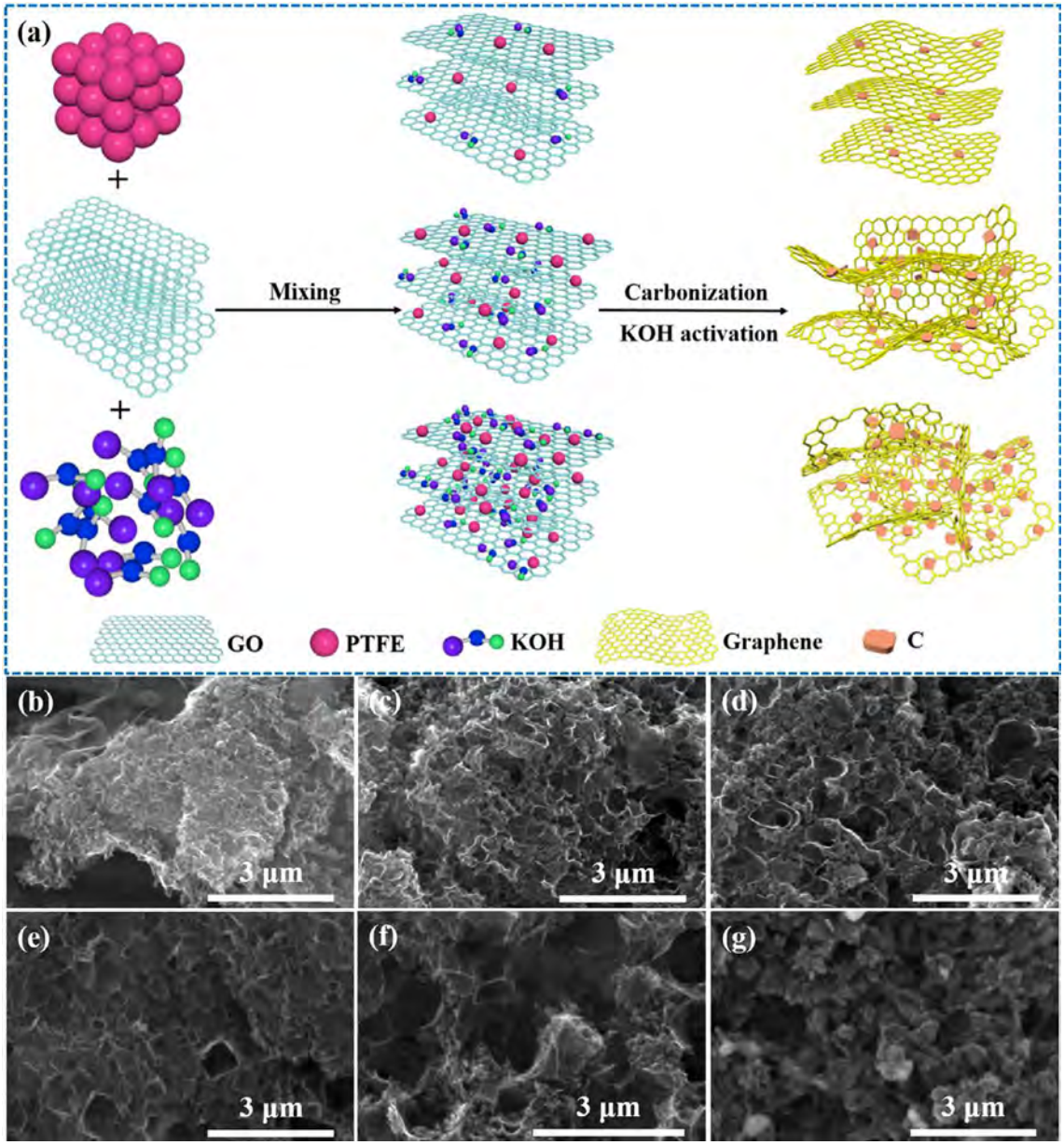

Fig. 1. (a) Schematic illustration for the prepare procedure of HPSNCs. SEM images of (b) HPSNC-1, (c) HPSNC-5, (d) HPSNC-10, (e) HPSNC-15, (f) HPSNC-20 and (g) pure PTFE derived nanocarbons.

PTFE obtained by KOH activation, the corresponding Raman spectroscopy was presented in Figs. 3(b) and S6. The *D*-band located at ~1350 cm^{-1} which was caused by structural defects and sp^3-hybridized bonds of carbon materials [34], and *G*-band located at ~1590 cm^{-1} was derived from the E_{2g} vibrational mode [35]. The values of I_D/I_G calculated from the area of *D*-band and *G*-band after multi-peak fitting through the Voigt function was widely used as an indicator of structural defects of carbon materials. Herein, the I_D/I_G values of the as-prepared HPSNC samples are 2.559 ± 0.128, 2.367 ± 0.164, 2.234 ± 0.083, 2.238 ± 0.040 and 2.365 ± 0.106 for HPSNC-1, HPSNC-5, HPSNC-10, HPSNC-15 and HPSNC-20, respectively (SI, Table S1), which implies high ratio of defects. And the effective crystallite sizes L_a in the direction of the graphite plane are also listed (SI, Table S1).

To detect the compositions and the chemical binding of the HPSNC samples, XPS analysis was performed. The atom percentage of Carbon element is higher than 94%, Oxygen element varies from 3.0 to 5.9%, and no any Fluorine and Potassium elements were detected by XPS survey (Fig. 3c and Table S2), which implies that the PTFE powders were completely transformed and/or ignited. One typical deconvolution curve of C1s spectrum for HPSNC-15 is shown in Fig. 3d and the others are also discussed (SI, Fig. S7). One strong peak locating at 284.78 eV in C1 s spectra ascribes to sp^2 carbon and some accompanied peaks occurred at 285.80, 287.10 and 289.8 eV can be ascribed to C–OH, C=O and COOH, respectively (SI, Table S3) [8,36]. These results demonstrate that GO is effectively thermally reduced and PTFE powders are successfully transformed into low heteroatoms functionalized nanocarbons.

The pore structure characteristics of the as-prepared HPSNC samples with different ratios of GO to PTFE were investigated by using surface area analysis. The N_2 adsorption/desorption isotherms and interrelated pore size distribution curves were shown in Fig. 4a–b. The related parameters obtained from the isotherms are also listed in Table S4. It can be seen that all the isotherms are typical type IV according to the IUPAC classification, which

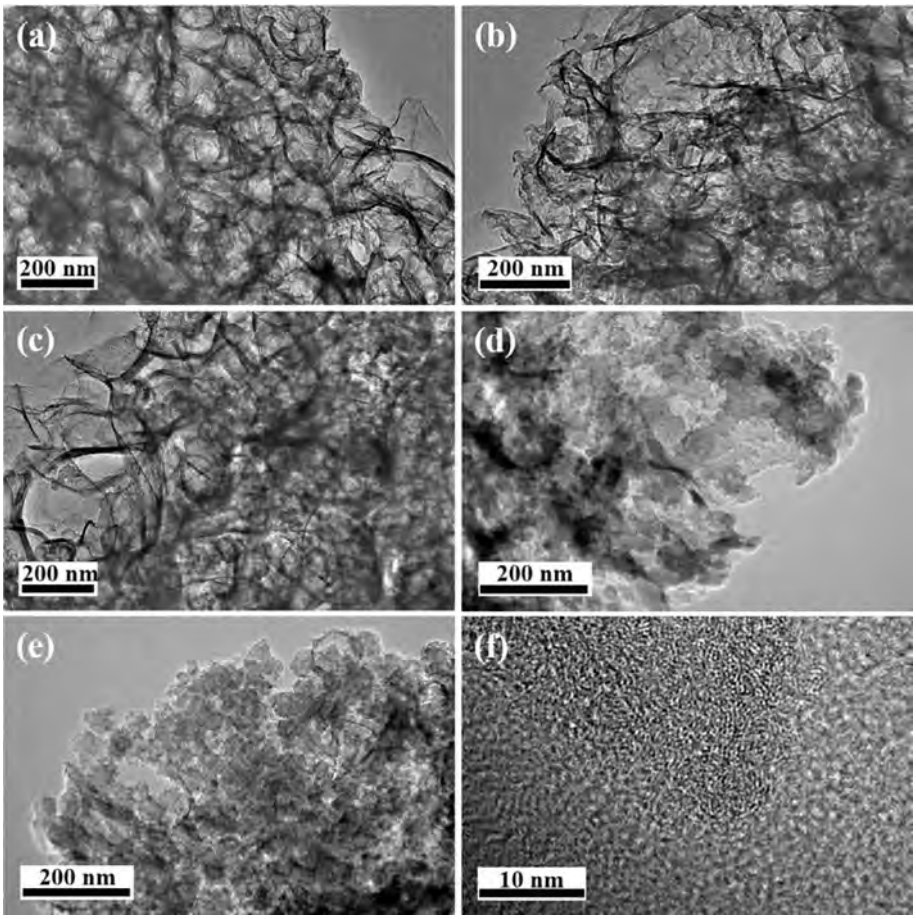

Fig. 2. TEM images of (a) HPSNC-1, (b) HPSNC-5, (c) HPSNC-10, (d) HPSNC-15, (e) HPSNC-20 and (f) HRTEM image of HPSNC-15.

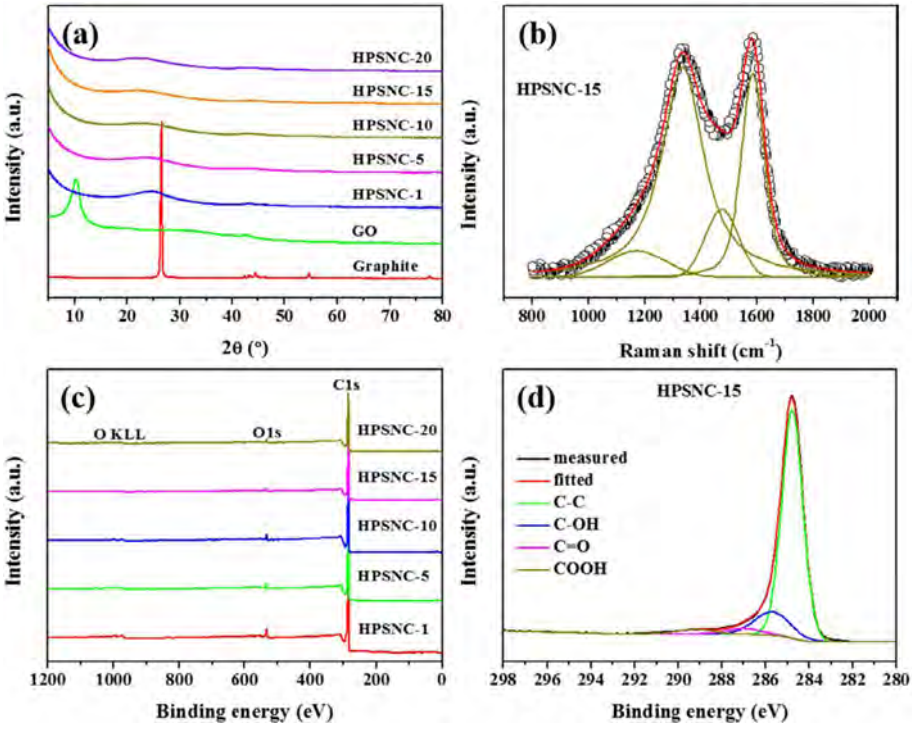

Fig. 3. (a) XRD patterns of graphite, GO and the as-prepared HPSNC samples. (b) Raman spectra of one typical HPSNC-15 sample. (c) XPS of the as-prepared HPSNCs and (d) Deconvolution curves of C1s for HPSNC-15.

indicates the existence of various pore sizes from micropores to macropores. The SSA desirably increases with the increasing weight ratio of GO to PTFE from 1: 1 to 1: 10. For the as-prepared HPSNC-1, the SSA value is only 880 $m^2 g^{-1}$, which is smaller than the as-prepared HPSNC-5 and HPSNC-10 (1156 $m^2 g^{-1}$ and 1992 $m^2 g^{-1}$, respectively). And the as-prepared HPSNC-10 has a higher total pore volume of 1.90 $cm^3 g^{-1}$ with a micropore volume of 0.51 $cm^3 g^{-1}$. What's more, the HPSNC samples present the exactly hierarchical porosity as exhibited in Fig. 4b, which supports the rapid channels for transport and migration of electrolyte ions. For clearly describing the unique structure, a schematic illustration of electrolyte solution storage in macropores and shortened ion transfer into mesopores and micropores is shown in Fig. 4c.

From the above-mentioned analysis, we can see that the as-prepared HPSNCs with unique microstructure and high SSAs can be considered as a promising electrode material candidate for supercapacitors. To investigate the electrochemical performance of as-prepared HPSNC samples, we have fabricated a two-electrode symmetric configuration using $EMIMBF_4$ as the electrolyte, and the results are shown in Fig. 5. The values of specific capacitance for HPSNCs are presented in Fig. 5a with the current densities varying from 0.2 A g^{-1} to 20 A g^{-1}, which were calculated using their galvanostatic discharge curves. The HPSNC-15 possesses the highest specific capacitance at all applied current densities comparing with other electrodes. The maximum specific capacitance for HPSNC-15 is 39.5 F g^{-1} (158.1 F g^{-1} for a single electrode) at 0.2 A g^{-1}, and the specific capacitance gradually decreases with increasing current densities. Strikingly, it still maintains 76.9% capacitance retention (that is 30.4 F g^{-1} at a high current density of 20 A g^{-1}), indicating HPSNC-15 has superior rate capability. In addition, the HPSNC-1 HPSNC-5, HPSNC-10 and HPSNC-20 also show good rate-capability. The specific capacitance of HPSNC-1, HPSNC-5, HPSNC-10 and HPSNC-20 were 28.8, 34.7, 38.2, and 37.3 F g^{-1} at 0.2 A g^{-1} and maintains 21.0, 25.8, 30.2, and 27.1 F g^{-1} at a high current density of 20 A g^{-1}, indicating 72.9%, 74.4%, 79.1% and 72.7% capacitance retentions. In addition, HPSNC supercapacitors possess a high areal capacitance of ~400 mF cm^{-2} (Fig. 5b). Fig. 5c shows the GCD curves at a current density of 1 A g^{-1}. These curves with the work potential up to 3.5 V show exactly triangle-like shape, indicating good electric double layer capacitive behavior. Moreover, the linear GCD curves and low IR drop in Fig. S8 can be observed at high current densities, which also demonstrated the excellent rate-capability of HPSNC supercapacitors.

Fig. 5d shows the CV curves of HPSNC-15 at scan rates varying from 50 to 1000 mV s^{-1}. Clearly, the CV curves show a rectangular shape at relatively low scan rates, indicating electric double layer capacitance. It is fascinating that even at a fast scan rate of 1000 mV s^{-1}, the supercapacitors remain a nearly rectangular shape, which implies that the electroadsorption kinetics process is not largely limited. Furthermore, the CV curves of the HPSNC-1 HPSNC-5, HPSNC-10 and HPSNC-20 also exhibit in Fig. S9. The three-electrode configuration and symmetric supercapacitors were assembled with 6 M KOH as the electrolyte. Electrodes are based on HPSNC-1, HPSNC-5, HPSNC-10, HPSNC-15 and HPSNC-20. We have proved that the obtained HPSNC samples display excellent electrochemical performance in 6 M KOH aqueous solution (Figs. S10–11). HPSNC-15 possesses higher capacitance comparing with HPSNC-1, HPSNC-5, HPSNC-10 and HPSNC-20. HPSNC-15 electrode exhibits the maximum capacitance of 215.6 F g^{-1} at a high current density of 50 A g^{-1} in three-electrode configuration (Fig. S10c) and 36.5 F g^{-1} at 30 A g^{-1} in a two-electrode system (Fig. S11d). In contrast, the specific capacitance of pure PTFE derived nanocarbons is much lower than the HPSNCs. What's worse, the capacitance behavior is also deteriorated especially at low work voltage and low frequency (Fig. S12), which probably ascribes to its poor conductivity.

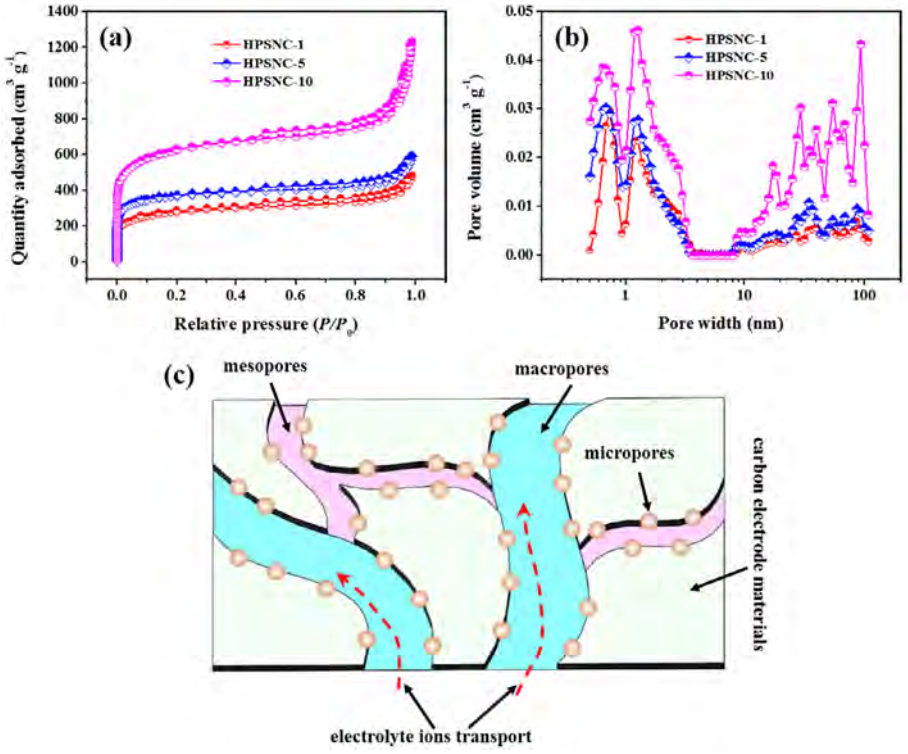

Fig. 4. (a) N_2 adsorption/desorption isotherms. (b) Pore size distribution curves. (c) Schematic illustration for the pore structure of the as-prepared HPSNC samples.

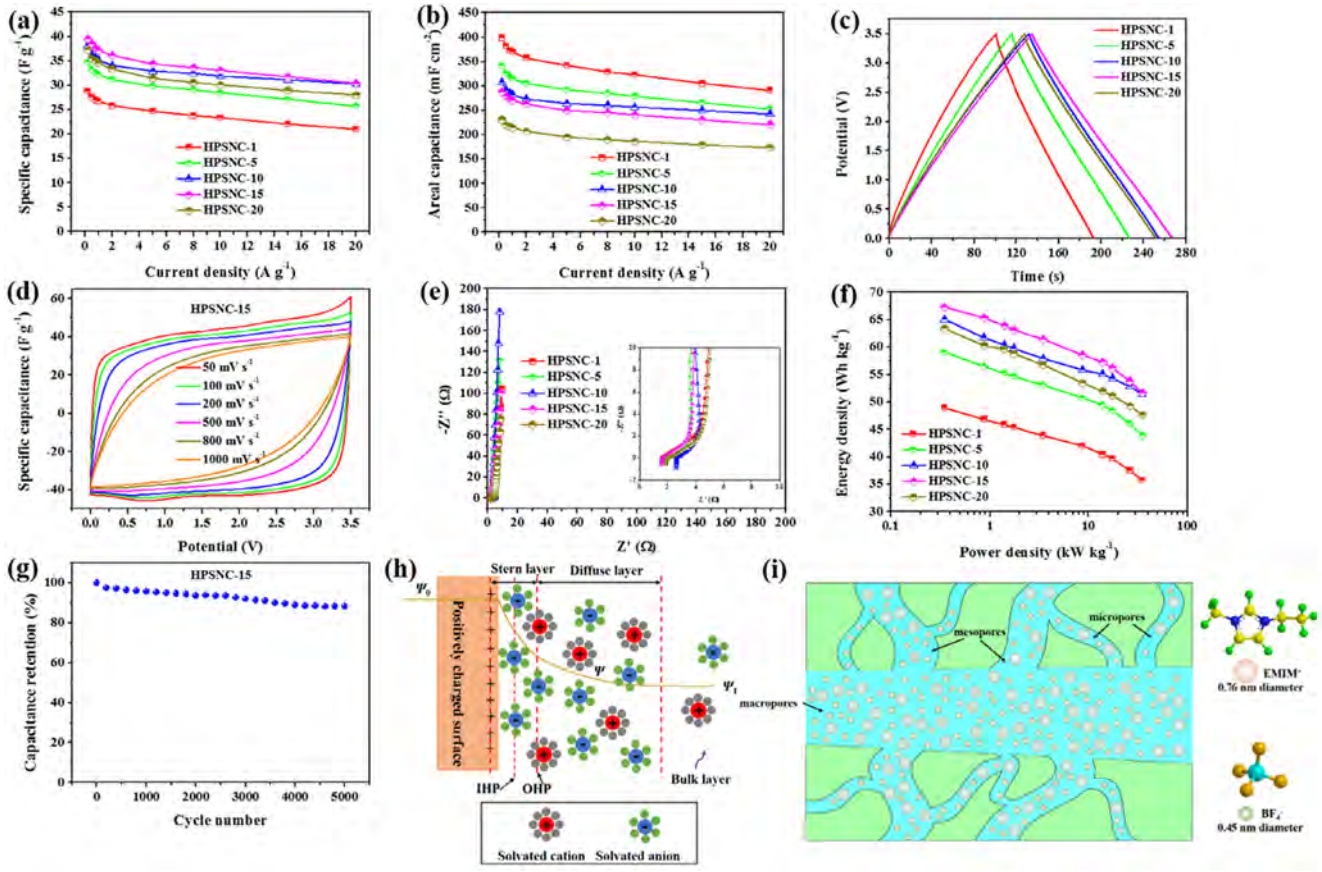

Fig. 5. Electrochemical performances of the HPSNC-based symmetrical supercapacitors in $EMIMBF_4$ IL electrolyte. (a) The specific capacitance values at different current densities. (b) The areal capacitance values at different current densities. (c) A comparison of the GCD curves at 1 A g^{-1}. (d) CV curves of HPSNC-15 at different scan rates. (e) Nyquist plots and the inset shows the magnified part of Nyquist plots at high frequency. (f) Ragone plots. (g) Cycling stability of HPSNC-15. (h) Electrical double-layer (EDL) model at a positively charged surface, Ψ_0, Ψ, Ψ_1 are the electrical potential at the electrode surface, electrode/electrolyte interface and bulk electrolyte, respectively. (i) Schematic illustration of the transport of $EMIMBF_4$ electrolyte ions in HPSNC electrodes.

Besides the capacitance, the resistance like ESR, Warburg, and equivalent distributed resistance (EDR) are other most important parameters of the supercapacitors. Fig. 5e presents the Nyquist plots of HPSNC-based symmetrical supercapacitors in the frequency ranges from 100 kHz to 10 mHz under AC voltage amplitude of 5 mV. It clearly shows that all the HPSNC devices exhibit a vertical line at the low frequency, indicating a good electric double layer capacitance. By the way, the imaginary resistance is larger for HPSNC-15 than that of HPSNC-1, HPSNC-5, and HPSNC-10, which ascribes to lighter mass of the former (1.82 ± 0.03 mg cm^{-2} for HPSNC-15, and 3.46 ± 0.04, 2.45 ± 0.05, 2.01 ± 0.08 mg cm^{-2} for HPSNC-1, HPSNC-5, and HPSNC-10). The ESR determined by the resistances of the electrode materials, the electrolyte, the interface, and the contact are as low as 1.7, 2.0, 2.7, 2.2, and 1.7 Ω for HPSNC-1, HPSNC-5, HPSNC-10, HPSNC-15 and HPSNC-20, respectively. Strikingly, the EDR are 2.7 Ω for HPSNC-1, 1.4 Ω for HPSNC-5, 1.1 Ω for HPSNC-10, 1.3 Ω for HPSNC-15 and 2.8 Ω for HPSNC-20 according to a method suggested by Kötz et al. [37], which means that the diffusion resistance is much smaller for HPSNC-10 with abundant pores in meso-to-macro-scales.

As shown in Fig. 5f, the Ragone plot of HPSNC-15 based symmetrical supercapacitor presents a high energy density of 67.3 Wh kg^{-1} at a power density of 0.35 kW kg^{-1}, and still remains 51.7 Wh kg^{-1} at a considerably high power density of 35 kW kg^{-1}, which shows much more superior performance than mostly previously reported nanocarbons based supercapacitors with $EMIMBF_4$ electrolyte (Table S5). Fig. 5g reveals a plot of the capacitance retention as a function of cycle number for HPSNC-15 based symmetrical supercapacitors at a current density of 5 A g^{-1}, the specific capacitance declines slightly and after 5000 cycling, 88% capacitance is still retained, revealing good cycle stability.

EDLCs can deliver outstanding power thanks to fast kinetics associated with the electrochemical storage mechanisms at the electrode-electrolyte interface as illustrated in Fig. 5h. Since the ion diffusivity is typically around seven orders of magnitude lower in solids than in liquids, the traditional porous materials like activated carbons and mesoporous carbons can fast establish EDL capacitance at only the interface near the electrolyte while the electroadsorption kinetics are severely inhibited as the electrode layer is far away from the electrolytes. There are some advantages through hierarchical porosity design to improve the electrochemical properties as indicated in Fig. 5i. Firstly, the macropores as ion-buffering reservoirs can largely shorten the transfer and diffuse distance of electrolyte ions into the mesopores and micropores, which is capable of overcoming the primary kinetic limits of electrochemical processes in porous electrodes [9,26,38]. Secondly, the ion-accessible surface areas are greatly increased as much more ions can form EDL interface inside the meso-to-micro-pores, which are critical to high SSA electrode materials [8,27]. More importantly, bulk materials with hierarchical porosity design still maintain relatively high density and good electric conductivity, which can avoid the occurrence of high weight capacitance and energy but extremely low when evaluated by volume [22,39–41]. Consequently, both high energy and power supercapacitors can be anticipated through unique porosity design.

4. Conclusions

In summary, we have demonstrated that sheet-like nanocarbons with hierarchically porous structure and high surface area can be simply prepared by direct KOH activation of graphene oxide and PTFE, in which PTFE was used as spacers and carbon sources. Through modifying the weight ratio of GO to PTFE, sheet-like nanocarbons with surface area ranging from 880 to 1992 $m^2 g^{-1}$ and pore volume from 0.74 to 1.90 $cm^3 g^{-1}$ have been obtained. The sheet-like nanocarbons with hierarchal porosity exhibit excellent electrochemical performance in $EMIMBF_4$ IL electrolyte as well as in KOH aqueous electrolyte. High energy density of 51.7 Wh kg^{-1} is obtained along with a high power density of 35 kW kg^{-1}, evidently demonstrating that hierarchically porous sheet-like nanocarbons can be considered as a promising candidate for both high energy and power supercapacitors. Also, this work opens up a new method to produce hierarchically porous structures for unique application.

Acknowledgements

This work was supported by the National Natural Science Foundation of China (No. 51602265), the Scientific and Technological Projects for Distinguished Young Scholars of Sichuan Province (No. 2015JQ0013), China Postdoctoral Science Foundation (No. 2016M592692), the Fundamental Research Funds for the Central Universities of China (No. A0920502051619-72) and the Independent Research Project of State Key Laboratory of Traction Power (Nos. 2017TPL_Z04, 2016TPL_Z03).

Appendix A. Supplementary data

Supplementary data associated with this article can be found, in the online version, at http://dx.doi.org/10.1016/j.cej.2017.04.012.

References

[1] P. Huang, C. Lethien, S. Pinaud, K. Brousse, R. Laloo, V. Turq, M. Respaud, A. Demortière, B. Daffos, P.L. Taberna, B. Chaudret, Y. Gogotsi, P. Simon, On-chip and freestanding elastic carbon films for micro-supercapacitors, Science 351 (2016) 691–695.
[2] Z. Yu, L. Tetard, L. Zhai, J. Thomas, Supercapacitor electrode materials: nanostructures from 0 to 3 dimensions, Energy Environ. Sci. 8 (2015) 702–730.
[3] Y. Shao, M.F. El-Kady, L.J. Wang, Q. Zhang, Y. Li, H. Wang, M.F. Mousavi, R.B. Kaner, Graphene-based materials for flexible supercapacitors, Chem. Soc. Rev. 44 (2015) 3639–3665.
[4] J. Vatamanu, D. Bedrov, Capacitive energy storage: current and future challenges, J. Phys. Chem. Lett. 6 (2015) 3594–3609.
[5] H. Zhang, X. Zhang, H. Lin, K. Wang, X. Sun, N. Xu, C. Li, Y. Ma, Graphene and maghemite composites based supercapacitors delivering high volumetric capacitance and extraordinary cycling stability, Electrochim. Acta 156 (2015) 70–76.
[6] H. Zhang, H. Su, L. Zhang, B. Zhang, F. Chun, X. Chu, W. He, W. Yang, Flexible supercapacitors with high areal capacitance based on hierarchical carbon tubular nanostructures, J. Power Sources 331 (2016) 332–339.
[7] M. Kim, Y. Hwang, J. Kim, Process dependent graphene/MnO_2 composites for supercapacitors, Chem. Eng. J. 230 (2013) 482–490.
[8] H. Zhang, X. Zhang, Y. Ma, Enhanced capacitance supercapacitor electrodes from porous carbons with high mesoporous volume, Electrochim. Acta 184 (2015) 347–355.
[9] H. Zhang, L. Zhang, J. Chen, H. Su, F. Liu, W. Yang, One-step synthesis of hierarchically porous carbons for high-performance electric double layer supercapacitors, J. Power Sources 315 (2016) 120–126.
[10] J. Chmiola, G. Yushin, Y. Gogosti, C. Portet, P. Simon, P.L. Taberna, Anomalous increase in carbon capacitance at pore sizes less than 1 nanometer, Science 313 (2006) 1760–1763.
[11] Y. Zhu, S. Murali, M.D. Stoller, K.J. Ganesh, W. Cai, P.J. Ferreira, A. Pirkle, R.M. Wallace, K.A. Cychosz, M. Thommes, D. Su, E.A. Stach, R.S. Ruoff, Carbon-based supercapacitors produced by activation of graphene, Science 332 (2011) 1537–1541.
[12] H. Zhang, K. Wang, X. Zhang, H. Lin, X. Sun, C. Li, Y. Ma, Self-generating graphene and porous nanocarbon composites for capacitive energy storage, J. Mater. Chem. A 3 (2015) 11277–11286.
[13] D. Yu, K. Goh, H. Wang, L. Wei, W. Jiang, Q. Zhang, L. Dai, Y. Chen, Scalable synthesis of hierarchically structured carbon nanotube-graphene fibres for capacitive energy storage, Nat. Nanotechnol. 9 (2014) 555–562.
[14] T. Lin, I.W. Chen, F. Liu, C. Yang, H. Bi, F. Xu, F. Huang, Nitrogen-doped mesoporous carbon of extraordinary capacitance for electrochemical energy storage, Science 350 (2015) 1508–1513.
[15] H. Zhang, X. Zhang, X. Sun, Y. Ma, Shape-controlled synthesis of nanocarbons through direct conversion of carbon dioxide, Sci. Rep. 3 (2013) 3534.
[16] H. Zhang, X. Zhang, X. Sun, D. Zhang, H. Lin, C. Wang, H. Wang, Y. Ma, Large-scale production of nanographene sheets with a controlled mesoporous architecture as high-performance electrochemical electrode materials, ChemSusChem 6 (2013) 1084–1090.
[17] X. Yang, C. Cheng, Y. Wang, L. Qiu, D. Li, Liquid-mediated dense integration of graphene materials for compact capacitive energy storage, Science 341 (2013) 534–537.
[18] Y.J. Kim, C.M. Yang, K.C. Park, K. Kaneko, Y.A. Kim, M. Noguchi, T. Fujino, S. Oyama, M. Endo, Edge-enriched, porous carbon-based, high energy density supercapacitors for hybrid electric vehicles, ChemSusChem 5 (2012) 535–541.
[19] L. Zhang, T. You, T. Zhou, X. Zhou, F. Xu, Interconnected hierarchical porous carbon from lignin-derived byproducts of bioethanol production for ultra-high performance supercapacitors, ACS Appl. Mater. Interfaces 8 (2016) 13918–13925.
[20] Y. Chen, X. Zhang, H. Zhang, X. Sun, D. Zhang, Y. Ma, High-performance supercapacitors based on a graphene-activated carbon composite prepared by chemical activation, RSC Adv. 2 (2012) 7747–7753.
[21] W. Tian, Q. Gao, L. Zhang, C. Yang, Z. Li, Y. Tan, W. Qian, H. Zhang, Renewable graphene-like nitrogen-doped carbon nanosheets as supercapacitor electrodes with integrated high energy-power properties, J. Mater. Chem. A 4 (2016) 8690–8699.
[22] Q. Shao, J. Tang, Y. Lin, J. Li, F. Qin, J. Yuan, L.C. Qin, Carbon nanotube spaced graphene aerogels with enhanced capacitance in aqueous and ionic liquid electrolytes, J. Power Sources 278 (2015) 751–759.
[23] D. Lozano-Castelló, D. Cazorla-Amorós, A. Linares-Solano, S. Shiraishi, H. Kurihara, A. Oya, Influence of pore structure and surface chemistry on electric double layer capacitance in non-aqueous electrolyte, Carbon 41 (2003) 1765–1775.
[24] R. Mysyk, E. Raymundo-Piñero, J. Pernak, F. Béguin, Confinement of symmetric tetraalkylammonium ions in nanoporous carbon electrodes of electric double-layer capacitors, J. Phys. Chem. C 113 (2009) 13443–13449.
[25] J.W. Graydon, M. Panjehshahi, D.W. Kirk, Charge redistribution and ionic mobility in the micropores of supercapacitors, J. Power Sources 245 (2014) 822–829.
[26] D.W. Wang, F. Li, M. Liu, G.Q. Lu, H.M. Cheng, 3D aperiodic hierarchical porous graphitic carbon material for high-rate electrochemical capacitive energy storage, Angew. Chem. 120 (2008) 379–382.
[27] L. Zhang, X. Yang, F. Zhang, G. Long, T. Zhang, K. Leng, Y. Zhang, Y. Huang, Y. Ma, M. Zhang, Y. Chen, Controlling the effective surface area and pore size distribution of sp^2 carbon materials and their impact on the capacitance performance of these materials, J. Am. Chem. Soc. 135 (2013) 5921–5929.
[28] E. Mourad, L. Coustan, P. Lannelongue, D. Zigah, A. Mehdi, A. Vioux, S.A. Freunberger, F. Favier, O. Fontaine, Biredox ionic liquids with solid-like redox density in the liquid state for high-energy supercapacitors, Nat. Mater. (2016), http://dx.doi.org/10.1038/nmat4808.
[29] H. Zhang, X. Zhang, D. Zhang, X. Sun, H. Lin, C. Wang, Y. Ma, One-step electrophoretic deposition of reduced graphene oxide and $Ni(OH)_2$ composite films for controlled syntheses supercapacitor electrodes, J. Phys. Chem. B 117 (2013) 1616–1627.
[30] D.P. Serrano, J.M. Escola, P. Pizarro, Synthesis strategies in the search for hierarchical zeolites, Chem. Soc. Rev. 42 (2013) 4004–4035.
[31] J. Xiao, D. Mei, X. Li, W. Xu, D. Wang, G.L. Graff, W.D. Bennett, Z. Nie, L.V. Saraf, I.A. Aksay, J. Liu, J.G. Zhang, Hierarchically porous graphene as a lithium–air battery electrode, Nano Lett. 11 (2011) 5071–5078.
[32] Y.Y. Peng, Y.M. Liu, J.K. Chang, C.H. Wu, M.D. Ger, N.W. Pu, C.L. Chang, A facile approach to produce holey graphene and its application in supercapacitors, Carbon 81 (2015) 347–356.
[33] J. Xu, Z. Tan, W. Zeng, G. Chen, S. Wu, Y. Zhao, K. Ni, Z. Tao, M. Ikram, H. Ji, Y. Zhu, A hierarchical carbon derived from sponge-templated activation of graphene oxide for high-performance supercapacitor electrodes, Adv. Mater. 28 (2016) 5222–5228.
[34] C. Zheng, X.F. Zhou, H.L. Cao, G.H. Wang, Z.P. Liu, Controllable synthesis of activated graphene and its application in supercapacitors, J. Mater. Chem. A 3 (2015) 9543–9549.
[35] Q. Zhou, X. Ye, Z. Wan, C. Jia, A three-dimensional flexible supercapacitor with enhanced performance based on lightweight, conductive graphene-cotton fabric electrode, J. Power Sources 296 (2015) 186–196.
[36] S. Wu, G. Chen, N.Y. Kim, K. Ni, W. Zeng, Y. Zhao, Z. Tao, H. Ji, Z. Lee, Y. Zhu, Creating pores on graphene platelets by low-temperature KOH activation for enhanced electrochemical performance, Small 12 (2016) 2376–2384.
[37] D. Weingarth, D. Cericola, F.C.F. Mornaghini, T. Hucke, R. Kötz, Carbon additives for electrical double layer capacitor electrodes, J. Power Sources 266 (2014) 475–480.
[38] J. Chmiola, C. Largeot, P.L. Taberna, P. Simon, Y. Gogotsi, Desolvation of ions in subnanometer pores and its effect on capacitance and double-layer theory, Angew. Chem. 120 (2008) 3440–3443.
[39] D.N. Futaba, K. Hata, T. Yamada, T. Hiraoka, Y. Hayamizu, Y. Kakudate, O. Tanaike, H. Hatori, M. Yumura, S. Iijima, Shape-engineerable and highly

densely packed single-walled carbon nanotubes and their application as super-capacitor electrodes, Nat. Mater. 5 (2006) 987–994.
[40] Z.Y. Sui, Y.N. Meng, P.W. Xiao, Z.Q. Zhao, Z.X. Wei, B.H. Han, Nitrogen-doped graphene aerogels as efficient supercapacitor electrodes and gas adsorbents, ACS Appl. Mater. Interfaces 7 (2015) 1431–1438.
[41] C. Ma, J. Sheng, C. Ma, R. Wang, J. Liu, Z. Xie, J. Shi, High-performanced supercapacitor based mesoporous carbon nanofibers with oriented mesopores parallel to axial direction, Chem. Eng. J. 304 (2016) 587–593.